ACS Catalysis

Universitat d'Alacant
Universidad de Alicante

Subscriber access provided by Universidad de Alicante

Article

On the reaction mechanism for oxygen reduction on platinum: Existence of a fast initial chemical step and a soluble species different to H2O2

Ana Maria Gomez-Marín, Juan M. Feliu, and Edson A. Ticianelli

ACS Catal., **Just Accepted Manuscript** • DOI: 10.1021/acscatal.8b01291 • Publication Date (Web): 19 Jul 2018

ACS Publications

is published by the American Chemical Society. 1155 Sixteenth Street N.W., Washington, DC 20036

On the reaction mechanism for oxygen reduction on platinum: Existence of a fast initial chemical step and a soluble species different to H_2O_2

Gómez–Marín, Ana[1,2,*], Feliu, Juan[3,*], Ticianelli, Edson[1]

[1] Instituto de Química de São Carlos, Universidade de São Paulo, Caixa Postal 780, Fisico Quimica, Av. Trabalhador Sao Carlense, São Carlos CEP 13560-970, SP, Brazil.

[2] Department of Chemistry, Division of Fundamental Sciences (IEF), Technological Institute of Aeronautics (ITA), Zip Code: 12228-900, SP, Brazil.

[3] Instituto de Electroquímica, Universidad de Alicante, Apt 99, E-03080 Alicante, Spain.

* E-mail: amgomezma@usp.br (A.M. Gómez–Marín), juan.feliu@ua.es (J.M. Feliu).

Abstract

The oxygen reduction reaction (ORR) on platinum in perchloric acid is studied under transient conditions at stationary and non-stationary electrodes. Only under these conditions, the presence of a fast initial chemical step in the mechanism, giving rise to a soluble, short-lived intermediate proposed to be the HO_2^* radical, is revealed, by comparing experimental and calculated curves by numerical simulations of simple reaction schemes. The formation of this species and the existence of a zero-current cycle involving it would be the main reasons for the lack of reduction currents at potentials higher than the ORR reaction onset. Additionally, regardless of the exact subsequent steps after the initial chemical reaction, if HO_2^* is generated it would disproportionate to hydrogen peroxide, which implies that both species would be always produced during the ORR on Pt. The presence of HO_2^* and H_2O_2 would profoundly affect the durability of Pt-based catalysts and should be taken into account in the design of materials for fuel cell cathodes.

Keywords: Cyclic voltammetry, non-steady state, scan rate study, mass-transport effects, rotating disk electrodes, hydroperoxyl radical.

1. Introduction

Oxygen reduction reaction (ORR) is a fundamental process in electrochemistry and certainly, its sluggish kinetics is one of the main drawbacks for the large-scale commercialization of fuel cell technology. Despite decades of research, the reaction occurs at a significant rate only at high overpotentials, and the highest reported improvement in the activity is a ~100 mV reduction in the overpotential on Platinum-based alloys relative to Pt, the most active pure metal [1-3]. This fact is commonly attributed to an inhibiting role of surface oxygen-containing species, such as adsorbed oxygen, O_{ads}, and/or hydroxyl, OH_{ads} [1,2,4-10], though their exact nature has not been undoubtedly established yet [11-16].

One of the reasons for the slow progress in the ORR catalyst´s development is the poor detailed knowledge about its mechanism. Early studies at oxide-free polycrystalline platinum, Pt(poly), both in acid and alkaline solutions, suggested that oxygen reduces to water along two parallel pathways [1,5,6,17-22]. A direct four-electron route, without any detectable intermediate,

$$O_2 + 4H^+ + 4e^- \rightleftarrows 2H_2O \qquad (1)$$

and another two-stage, serial route, in which hydrogen peroxide is first formed as a stable intermediate in a two-electron transfer, Eqn. (2), and further partially reduced to H_2O [1,20-23], Eqn. (3), giving an effective number of transferred electrons, n_{eff}, lower than 4,

$$O_2 + 2H^+ + 2e^- \rightleftarrows H_2O_2 \qquad (2, -2)$$

$$H_2O_2 + 2H^+ + 2e^- \rightleftarrows 2H_2O \qquad (3)$$

In alkaline solutions both routes seem to occur at comparable rates [22,24], while in acid media the role of the serial route is still an open question. It has been generally proposed that H_2O_2 only appears when impurities from the solution are adsorbed on the electrode surface [7,20,21,24]. However, an increase in the H_2O_2 amount measured during studies at nanostructured dilute arrays of Pt nanoparticles, NPs, [8-10,25-30], has suggested the serial path as the main ORR route [25]. In this case, it has been proposed that either the stronger adsorption of O-containing species at NPs [8-10], or the mass-transport enhancement as the size of Pt NPs decreases [27,30,31] induces the decrease in n_{eff} from 4- to 2- electrons [25-30]. Nevertheless, because under high mass-transport rates impurity effects are important

even at ppb levels of solution contaminants [32], the decrease in n_{eff} may be still due to solution impurities and not caused by the actual ORR mechanism.

On the other hand, ORR studies at Pt(111) electrodes in acid media have also suggested the presence of a soluble intermediate, but in place of H_2O_2, the hydroperoxyl radical, HO_2^*, has been proposed to be the most probable species, Eqn. (4) [13,15,16,33,34].

$$O_2 + 2PtH_2O_{ads} \rightleftarrows PtOH_{ads} + PtHO^*_{2,ads} + H_2O \qquad (4)$$

A decrease in n_{eff} by increasing the mass-transport rate hints toward the existence of a chemical reaction inside the ORR mechanism [10,30,35-40]. If this were the case, currents in linear sweep voltammetry (LSV) should become independent of the scan rate, v, when the equivalent characteristic time of the sweep, τ_v, (*i.e.* the time during which a stable electroactive species can communicate with the electrode [31]) is shorter than the magnitude of the time scale of the chemical reaction [37,41-51]. At these v's, currents are "kinetic currents", controlled by the chemical process rather than the charge transfer [37,41-51], and would not follow the Randles–Ševčík equation for single charge transfers, Eqn. (5), or overall n-electron processes with a first electron transfer as rate-determining step (RDS) [31,37,41-46], as the ORR [1,5,6,17-22],

$$j_p = \chi_{max} nFAC_O^0 \left(\sqrt{\frac{n_a FDv}{RT}}\right) \qquad (5)$$

with j_p, the peak current in the LSV. n, the total number of transferred electrons. n_a, the number of transferred electrons in the RDS (usually one). F, the Faraday's constant. A, the electrode geometric area. C^0_O and D the solubility and the diffusion coefficient of the reactant in the electrolyte, respectively. R, the ideal gas constant, T the temperature, and χ_{max} a constant equal to 0.446 or $0.496\sqrt{\alpha}$ for fast or slow charge transfers, respectively, with α, the transfer coefficient.

Accordingly, if the decrease in n_{eff} at Pt NPs is a true kinetic response, and not produced by solution impurities, a similar decrease in n_{eff} should also occur during LSV on bulk electrodes at a particular v, fast enough for reaching the kinetic control by the chemical step [37,41-51]. The advantage of this approach, *i.e.* increasing v instead of reducing the nanoparticle size, stems on the possibility to differentiate diffusional from surface contamination effects, because at stationary and rotating disk electrodes (RDEs) at

conventional rotation rates, ω < 3600 rpm, solution purity requirements are easier to achieve. Besides, the influence of contamination can be reduced at increasing v´s.

Following this methodology the ORR on Pt(poly) is studied in this work. Results confirm the first electron transfer as the RDS and reveal the presence of chemical steps in the main ORR pathway, shedding light over a long-standing dilemma. According to simulated LSVs, experimental data can only be explained by considering an initial chemical step and the participation of a soluble intermediate species in the main ORR mechanism. However, contrary to what has been already suggested [25-30], the intermediate species is different to H_2O_2, although it could either reduce or disproportionate to H_2O_2 in a subsequent reaction. Hence, during the ORR both, inner- and outer-sphere reactions take place, and H_2O_2 would be always produced during the ORR on Pt.

2. Experimental

Electrochemical measurements were conducted at room temperature (RT), ~22 °C, in a two–compartment, three electrodes, all–glass cell, using an Autolab (Nova) potentiostat/galvanostat equipped with an interchangeable rotating platinum disk electrode setup (Pine Instruments). Suprapure perchloric acid (Merck) was used to prepare aqueous solutions in ultrapure water (Purelab Ultra, Elga–Vivendi). O_2 and Ar (N50, Air Liquid) were also employed. All potentials were measured against the Reversible Hydrogen Electrode (RHE) and a large, flame cleaned, Pt wire coil was used as a counter electrode. *In situ* IR drop corrections were also made to compensate the electrolyte resistance [31]. The stability of the voltammetric profiles with time was carefully checked to ensure solution cleanliness, especially during RDE experiments, due to the forced convection conditions.

A Platinum disk (5 mm diam., 0.196 cm^2), polished to a mirror finish before each experiment (0.3 μm alumina, Buehler), was employed. Before each experiment, the electrode was left in concentrated sulfonitric solution at least 24 h and generously washed with ultrapure water. Later, the disk was flame annealing followed by quenching in ultrapure water before being assembled into the RDE set up. Inside the cell, the electrode was electrochemically treated by several consecutive anodic and cathodic pulses (60 s each) at 1.4 and -0.25 V, respectively, followed by voltammetric cycles between -0.25 to 1.15 V

at 0.1 V s^{-1} until obtaining an stable and typical cyclic voltammogram (CV) between 0.05 to 1.15 V (Figure S1B). The electrode roughness factor, *i.e.* the ratio between the electrochemical active surface area (ECSA) and the geometric area of the electrode, was between ~1.2 to 1.3, calculated from the CV in Ar-saturated 0.1 M $HClO_4$ solutions and by considering one adsorbed monolayer equal to ~0.200 mC cm^{-2} [52,53].

Moreover, because transient experiments are very sensitive to initial conditions, as it will be discussed below, a conditioning program before each experiment was applied to the electrode to get quantifiable and reproducible data. The program was similar to the one already reported [54,55] and consisted in sweeping the electrode between 1.15 and -0.05 V at 0.5 V s^{-1} five times, beginning from the open circuit potential (OCP) in a O_2-saturated 0.1 M $HClO_4$ solution, ~1.02 V, in the positive-going direction, as it is shown in Fig. S1A. This procedure assures that the electrode surface is in a similar state before every measurement.

In order to provide a qualitative understanding of experimental results, CVs at RDEs for simple reaction schemes of reversible and irreversible charge transfers including chemical reactions were also calculated via digital simulation techniques, by using the general purpose, commercial software COMSOL Multiphysics® 5.1. Details regarding the implementation can be found in the software's reference manual and modules' user guides. Simulations have been performed with successive mesh refinement until no appreciable changes in the CV occurred in calculated curves.

For mathematical simplicity, the diffusion equation based on the Nernst model [56-60] is solved numerically. Under this model, all non-stationary processes are assumed to occur within a thin layer bounded to the electrode surface, the Nernst diffusion layer, of thickness δ_{diff}. Outside this layer, a fixed concentration for all species is assumed: $C\ (x = \delta_{diff}) = 0$ for all products, and $C\ (x = \delta_{diff}) = C^0_O$ for the reactant. The error induced by this procedure is smaller than 4% when calculating peak currents in CVs of single electron transfers, either reversible, irreversible, or quasi-reversible, at RDEs under non-steady state conditions [61]. Following Levich [62], the thickness of this steady-state diffusion layer at any rotation rate was calculated according to [31,62].

$$\delta_\omega = 1.612 D^{1/3} \upsilon^{1/6} \omega^{-1/2} \qquad (6)$$

with $\upsilon = 0.01009$ cm^2 s^{-1}, the kinematic viscosity of 0.1 M $HClO_4$ [7].

3. Results and discussion

3.1. ORR on Pt surfaces at high potentials ($j = 0$)

Right after the corresponding cleaning step, electrodes were characterized in Ar-saturated 0.1 M $HClO_4$, and afterwards the solution was saturated with O_2. Next, before performing any study, it was necessary to select a proper upper potential limit (E_{up}) that guarantees an equivalent initial state at each evaluated v. Here, E_{up} should be well positive to the foot of the wave to avoid any effect in the shape of the curve [42-46], but low enough to assure a constant ECSA [52,63,64], and a surface covered only by OH_{ads} and/or O_{ads}, and not by a true oxide [63-65]. This is because different ORR mechanisms are expected over oxide-free and oxidized surfaces [5,6]. The fulfillment of the two last requirements can be achieved by setting $E_{up} \leq 1.15$ V [63-65].

In the process of choosing E_{up}, it was found that if the ORR negative-going scan was recorded after holding the electrode for a time, τ_h, at a potential, $E_i \leq 1.15$ V, close to the reaction onset, E_{onset}^{ORR}, a continuous increase in the ORR peak current, j_p^{ORR} is measured until reaching a limiting value, $j_p^{ORR}{}_{lim}$. Figure 1A illustrates this point for $0 \leq \tau_h \leq 120$ s at the open circuit potential ($j = 0$) in O_2-saturated solutions (OCP, $E_i \sim 1.02$ V). Increasing τ_h, continuously enhances j_p^{ORR} up to a maximum value, $j_p^{ORR}{}_{lim}$, Fig. 1B. Although several measurements were taken for each point, error bars are only reported at $\tau_h = 150$ s in Figs. 1B and 1C, but they are similar in all cases.

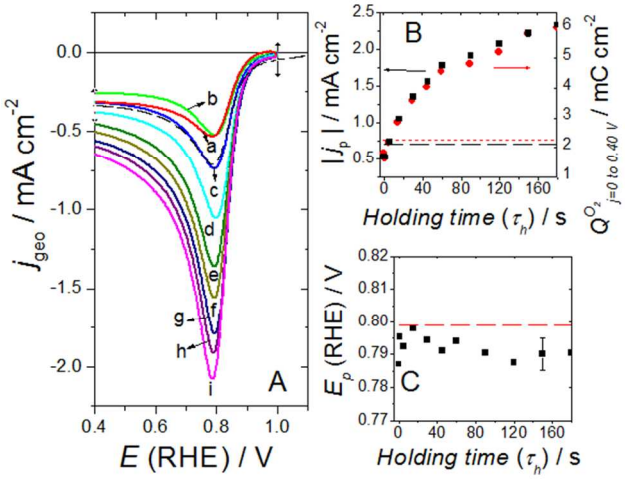

Figure 1: (A) Linear sweep voltammograms for the oxygen reduction in O_2-saturated 0.1 M $HClO_4$ on stationary Pt(poly) electrodes after conditioning and holding at E_i = 1.02 V (OCP) for different resting times, τ_h. a) 0, b) 1, c) 5, d) 15, e) 30, f) 45, g) 60, h) 90, i) 120 s and for the continuous LSV (dashed lines). (B) Absolute value of peak currents, j_p^{ORR}, (■, left), and total integrated reduction charge in j_p^{ORR} from j = 0 to E = 0.4 V, $Q_{tot}^{O_2}(\tau_h)$ (●, right), and (C) Peak potentials, E_p^{ORR}, as functions of τ_h. Dashed lines in (B) and (C) are the values during the continuous LSV. Scan rate 0.1 V s^{-1}.

This dynamics is also found if, instead of increasing τ_h at constant E_i as in Fig. 1, E_i is increased at constant τ_h. Then, similar to what has been reported for Pt(111) [13,34], it appears that j_p^{ORR} is a complex function of both τ_h and $E_i \geq E_{onset}^{ORR}$, despite the lack of reduction currents at these potentials that would indicate no apparent O_2 reduction. In fact, j_p^{ORR} is influenced even by the value of E_{up} in the "*continuous LSV*", since E_{up} indirectly determines the time spent by the electrode at $E_i \geq E_{onset}^{ORR}$. For example, j_p^{ORR} for the continuous LSV with E_{up} = 1.15 V in Fig. 1 (dashed curve) is similar to the measured j_p^{ORR} when the electrode is held at the OCP for 5 s, (curve *c*), although only ~3 s are necessary to go and return from 1.02 V to 1.15 V. Here, the subsequent third LSV scan after beginning the experiment is considered as the *continuous LSV* (see Fig. S1A).

The complex dependence of j_p^{ORR} on the time spent by the electrode at potentials higher than E_{onset}^{ORR} makes necessary imposing a conditioning procedure to the electrode before each experiment, in order to get comparable and reproducible data. In contrast, similar experiments but under steady state conditions (no peak in the LSV) only result in a shift toward negative potentials for E_{onset}^{ORR}, classically attributed to an inhibiting role of O_{ads}, and/or OH_{ads} species [1,2,4-10]. This result is rather unexpected because if O_2 does not react in a significant way at $E_i \geq E_{onset}^{ORR}$, as currently accepted [1-11,14,17-30,33,40,54,55,65,66-81], a constant j_p^{ORR} value, proportional to $C^0_{O_2}$ and independent of τ_h and E_i, as predicted by Eqn. (5), should have been measured.

In an attempt to explain the enhancement on j_p^{ORR} in Fig. 1, four possibilities were analyzed. The first one considers that results in Fig. 1 are caused by an incomplete recovery of the O_2-diffusion layer after the conditioning procedure, *i.e.* the O_2 concentration close to

the surface, C_{O_2} (x = 0), at τ_h = 0 is lower than the bulk concentration, $C^0_{O_2}$, but it approaches $C^0_{O_2}$ at increasing τ_h at E_i (*i.e.* it increases). However, by comparing τ_h and the characteristic time of the LSV, τ_v, it is realized that τ_v is always significantly smaller than τ_h at $E_i \geq$ OCP, curves *b* to *i* in Fig. 1A. Then, enough time has passed to recover the O_2-diffusion layer before j_p^{ORR} occurs, and, in absence of any reaction of O_2 at E_i, C_{O_2} (x = 0) should be equal to $C^0_{O_2}$. Worth mentioning that τ_v for v = 0.5 and 0.1 V s^{-1}, the scan rates of the conditioning procedure and the LSV in Fig. 1, are ~0.05 and ~ 0.26 s [31], respectively.

The second explored explanation was to analyze if results in Fig. 1A could come from a rise in the coverage of adsorbed O-containing species. It is well known that the coverage of these species raises at Pt(poly) surface when the electrode is held at E > 0.8 V [52,63,64,82,83]. Nevertheless, the total reduction charge transferred in j_p^{ORR}, estimated by integration of LSVs at any τ_h, $Q_{tot}^{O_2}(\tau_h)$, and given in Fig. 1B, (●, right), is always significantly greater than ~0.200 mC cm^{-2}, the reduction charge of adsorbed O-containing species in Ar-saturated solutions, $Q_{tot}^{Ar}(\tau_h)$, under equivalent experimental conditions [52,53,82,83]. Therefore, at constant ECSA, OH_{ads} and/or O_{ads} desorption cannot account for all the charge transferred in j_p^{ORR}, which varies from 1.5 to 6.0 mC cm^{-2} for an increase in τ_h from 0 to 180 s. In agreement with the reported negligible effect of O_2 on the Pt surface oxide formation, indicating identical coverages in N_2 and O_2 saturated solutions [83].

Indeed, a $Q_{tot}^{Ar}(\tau_h)$ ~2.5 mC cm^{-2} only could be measured in Ar-saturated electrolytes after the formation of a true-oxide phase on Pt(poly), due to the enhancement in the ECSA and it would require, at least, a $\tau_h > 5x10^3$ s at 2.2 V, or longer τ_h at lower potentials [63,64,82]. However, experimental conditions in Fig. 1A, guarantee a constant ECSA and the absence of a true-oxide phase, verified by both a constant integrated charge from the hydrogen adsorption/desorption region and the lack of any characteristic desorption peaks in the LSV attributable to the desorption of true Pt oxides [52,63,64,82]. Hence, analogous to what has been already reported for the ORR at Pt(111) [13], the raise in j_p^{ORR} cannot be explained by an increase in the coverage of adsorbed O-containing species.

The third examined interpretation was to contemplate a catalytic role of adsorbed O-containing species toward the ORR, in contrast to the poisoning character commonly

attributed to these species [1-2,4-7]. For this analysis, LSVs at RDEs at different rotation rates and *v*'s were taken and results are given in Figures 2 and S2. If any catalytic role of adsorbed species exists, a similar improvement in reduction currents should be also measured at RDEs when the potential is held at the OCP for 150 s (continuous line in Fig. 2) relative to the continuous LSV, at a given *v* and regardless of ω. Since the amount of O-containing species adsorbed on the electrode should not be affected by the mass transport under the same hydrodynamic conditions.

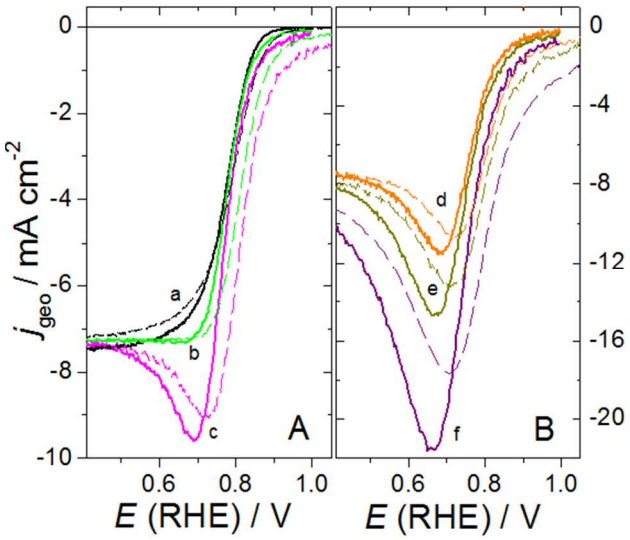

Figure 2: Linear sweep voltammograms for the ORR at Pt(poly) in O_2-saturated 0.1 M $HClO_4$ on RDEs at 2500 rpm after conditioning and holding the potential at E_i = OCP a resting time τ_h = 150 s. The scan rate in (A) is a) 0.1, b) 0.8, c) 2, and in (B) d) 3, e) 5, f) 10 V s^{-1}. For the sake of comparison continuous LSVs (dashed) are also given.

Contrarily, as it can be seen in Figs. 2 and S2, a rise in reduction currents by holding the potential at the OCP is only measured at RDEs on the subsequent LSVs that are under diffusional control, *i.e.* the ones at a scan rate fast enough relative to ω for j_p^{ORR} to appear. In this case, the magnitude of the current enhancement depends on *v* and ω. Besides, there is a negative shift in E_{onset}^{ORR} toward less positive potentials at any *v* when the potential is held at the OCP for 150 s (continuous line in Fig. 2) relative to the continuous LSV. All these results would support more an inhibiting than a catalytic role of O-containing species.

Alternatively, the necessity of a diffusional control for the increase in j_p^{ORR} to appear when the potential is held and the effect of the rotation rate in Figs. 1, 2 and S2 would indicate the involvement of a soluble species, in addition to O_2, rather than an adsorbed one. It is know that the flux of these species close to the surface is controlled by the magnitude of ω [31]. By considering this option, it is realized that results could be properly explained by an enrichment in the concentration of an electroactive species in the diffusion layer close to the surface, built up during the time the electrode was held at E_i.

This forth option would imply that dissolved oxygen reacted at $E_i > E_{onset}^{ORR}$, producing a soluble species, or an adsorbed one that may desorb and go into the solution. The magnitude of this reaction would depend on τ_h and E_i, as described above. If this were the case, the formed intermediate must accumulate and react, chemical and/or electrochemically, close to the surface until an equilibrium is reached, in such a way that no measurable reduction currents are recorded at $E_i > E_{onset}^{ORR}$ but, once the electrode potential reaches E_{onset}^{ORR}, its reduction gives rise to results in Figs. 1 and 2. Interaction with the water network will surely stabilize this species close to the surface, whose composition should certainly involve H and O atoms, allowing this water-like interaction.

Now, as reduction and oxidation reactions of H_2O_2 on Pt surfaces are relatively fast and only controlled by mass transport at low H_2O_2 concentrations [72,84,85], the intermediate responsible of results in Figs. 1 and 2 cannot be H_2O_2. First, because the fast H_2O_2 oxidation/reduction reaction kinetics would forbid the accumulation of H_2O_2. Second, because no equivalent increase in oxidation currents were measured when instead of a negative-, a positive-going scan was registered [86], as it is seen in Figure S3. If H_2O_2 had been accumulated close to the surface, an improvement in both reduction and oxidation currents would have been registered during the negative- and the positive-going scans, respectively, owing to the reduction/oxidation of the accumulated H_2O_2. Additionally, although H_2O_2 can disproportionate to O_2 and water, Eqn. (7), regenerating O_2 close to the surface [69-71], this perturbation in the diffusion layer cannot account for the dynamics seen in Figs. 1 and 2. The parallel production of water in Eqn. (7) would require the measurement of reduction currents at $E_i > E_{onset}^{ORR}$ if this reaction takes place [38,44,46,51,70,71],

$$H_2O_2 \rightleftarrows \frac{1}{2}O_2 + H_2O \qquad (7)$$

Furthermore, the fact that measurable oxidation currents at the ring of rotating ring-disk electrodes (RRDEs) at $E > 0.6$ V have been only reported during the ORR under high mass-transport conditions [8-10,27,30,31], indicates that the intermediate has a short lifetime and exists only within a thin reaction layer, δ_k, close to the Pt surface, $\delta_k << \delta_{diff}$. At mass-transport conditions typical of RRDEs, the species disappears before reaching the ring to be quantified [7,20,21,24,33]. In contrast, at high mass-transport conditions, such as those attained at microelectrodes [31,40] and on sparse arrays of Pt nanoparticles [8-10,27-30], the thickness of the Nernst diffusion layer could become thinner than δ_k, $\delta_k > \delta_{diff}$, at some conditions. In this latter case, the intermediate can go into the solution at measurable amounts before reacting with the electrode, or disproportioning to produce H_2O and O_2 as in Eqn. (7) [38,44,46,51,70,71], decreasing n_{eff} and making possible its detection by RRDEs, as it has been already reported [25-30].

In agreement with what it has been just discussed, oxidation currents close to E_{onset}^{ORR}, and with a maximum production close to the half-wave potential for the ORR, $E_{w/2}^{ORR}$, ~ 0.75 V, at stationary Pt(poly) in acid have been also reported by employing scanning electrochemical microscopy (SECM) [73]. This technique allows to measure closer to the surface than with a RRDE set up and thus, higher collection efficiencies can be attained [73,74]. Increasing oxidation currents have been also measured by SECM under transient conditions by closely approaching the electrode surface and right after a step from $E_i > E_{onset}^{ORR}$ to a potential in the diffusion controlled region, but only within the first 0.25 s and at small distances from the surface, ~ 4 to 12 μm [74]. These results are compatible with the existence of a short-lived intermediate species in a thin layer close to the surface.

3.2. Potentiodynamic response of the ORR on Pt surfaces

Qualitative investigations of electrochemical mechanisms are commonly performed by employing linear scan voltammetry, since by analyzing peak currents, j_p, as function of v, unusual current-potential, j-E, dynamics, relative to theoretical ones predicted by Eqn. 5, are easily detected [31,42-46,49,61]. Although this approach is usually performed with stationary electrodes, its extension to RDEs is qualitatively straightforward by a proper

adjustment of the system parameters, such as v and ω [37,46,50,56-59,61,87]. The main advantage of an hydrodynamic over a stationary technique stems on the suppression of natural convection effects, even at low values of the Reynolds number [56-59], opening the possibility to analyze the system under stable, and reproducible mass-transfer conditions [56-59,61,87].

Once initial conditions for a scan rate study are studied and the conditioning procedure to the electrode before each experiment defined, as shown in Fig. S1A, voltammograms at different scan rates at stationary and RDEs were taken, with E_{up} = 1.15 V and τ_h = 0 s. Here, because of the intrinsic dependence of j_p^{ORR} on E_{up} discussed above, the value of E_{up} selected was the highest potential that guarantees a $E_{up} > E_{onset}^{ORR}$ by at least 100 mV, a surface oxide film only composed by OH_{ads} and/or O_{ads} [63-65] and a constant ECSA [52,63,64] during experiments. In addition, RDEs were employed in an attempt to get information regarding the dynamics of the soluble intermediate described above, by fixing the maximum value of δ_{diff} that can be achieved, δ_ω, through the control of ω, according to Eqn. (6).

Figure 3 shows linear voltammetry scans, after background subtraction, for the oxygen reduction reaction on Pt(poly) at two different rotation rates, ω = 70 and 2500 rpm, and several scan rates. Besides, plots of normalized j_p, $i_p/nFAC^0_{O_2}\sqrt{D}$, against the normalized square root of the scan rate, $(\sqrt{\frac{n_a F v}{RT}})$, at the two rotating regimes, as well as at stationary electrodes are also given, Fig. 3C. These latter curves were calculated by considering D_{O_2} = $1.93x10^{-5}$ cm^2 s; $C^0_{O_2}$ = 1.26 mM; and $n = n_a = 1$. For the sake of comparison, theoretical curves for one, n = 1, and four, n = 4, fast and slow (α = 0.5) total charge transfers are also given.

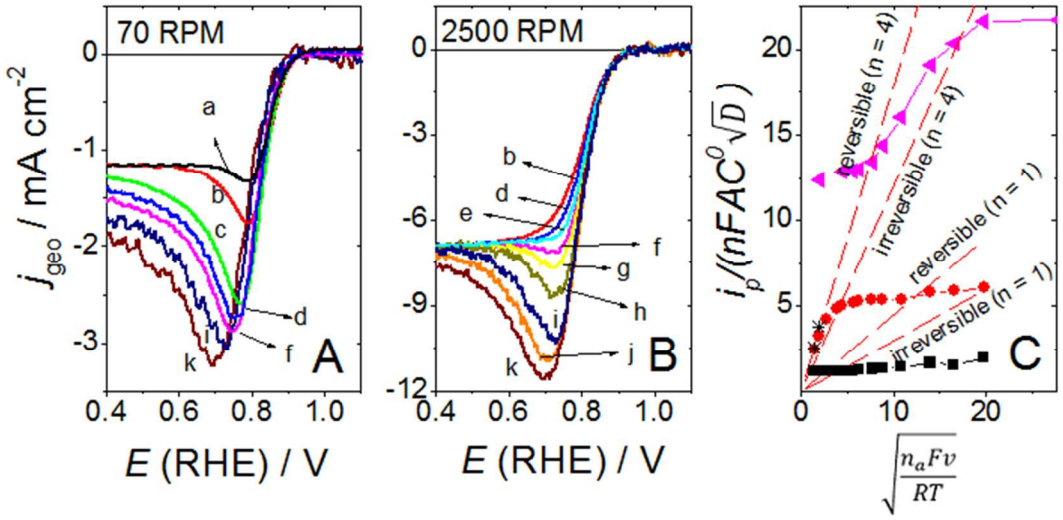

Figure 3: Background-subtracted negative-going scans at (A) 70 and (B) 2500 rpm for the oxygen reduction on Pt(poly) in O_2-saturated 0.1 M $HClO_4$ solutions after conditioning the electrode and two subsequent cyclic voltammograms. Scan rates are a) 0.05; b) 0.1; c) 0.4; d) 0.8; e) 1.0; f) 1.5; g) 2.0; h) 3.0; i) 5.0; j) 7.0; k) 10 V s^{-1}. (C) Normalized peak currents against the square root of the normalized scan rate at rotating disk electrodes: 70 (●) and 2500 rpm (◂), and at stationary electrodes: (■) continuous LSV and (ж) data from curve *i* in Fig. 1.

As it is appreciated, ORR polarization curves at RDEs are characterized either by a current peak, j_p, (Fig. 3A and curves *f* to *k*, Fig. 3B) or a limiting current, j_{lim}, (curves *b*, *d* and *e*, Fig. 3B) depending on the controlling mass-transport mode during the experiment [60]. In both cases, though, curves practically have comparable reaction onsets, suggesting the same RDS, except at the fastest scan rates at 70 rpm, $v > 3$ V s^{-1}, curves *i* and *k* in Fig. 3A.

When v is slow relative to ω, the time of the experiment is long enough for the concentration gradient in the solution to have a length such as that convection predominates over diffusion, $\delta_{diff} = \delta_{\omega}$. Under this hydrodynamic condition, a steady-state is achieved and *j-E* curves have the typical sigmoidal, S-shaped curves of convective systems, reaching a current plateau proportional to the square root of ω when the mass-transfer controlled

condition is attained (curves *b*, *d*, and *e*, Fig. 3B), as predicted by Levich equation [31,37,46,50,56-59,61,62],

$$j_{lim} = n_{eff} F A C^0_{O_2} \frac{D}{\delta_\omega} \qquad (8a)$$

where δ_ω is given by Eqn. (6), and so,

$$j_{lim} = 0.62 n_{eff} F A D^{2/3} \upsilon^{-1/6} C^0_{O_2} \omega^{1/2} \qquad (8b)$$

Typical kinetic analysis of steady-state curves at different ω, Figure 4, indicate a first-order dependence relative to $C^0_{O_2}$, and a change in the Tafel slope in the positive-going scan, from ~120 to 60 mV at high and low current densities, respectively, Fig. 4B, as commonly reported [1-3,5-16,17-19,25,26,33,72,76-78]. Instead, in the negative-going scan, Fig. 4C, a unique Tafel slope of ~70 mV is calculated. In Figs. 4B and 4C Tafel slopes were estimated as the inverse of the slope of a plot of the logarithm of kinetic currents, I_k, (calculated from experimental steady-state polarization curves at different ω [31]) as a function of the potential [31,56-59,61,62]. In the same way, limiting current densities are recorded at E < ~0.75 V, Figs. 3B and 4A, and the plot of $|j_{lim}|$ *vs.* $\omega^{1/2}$ (a Levich plot), given in Fig. 4D, follows a straight line with practically a zero intercept, as predicted by Eqns. (8).

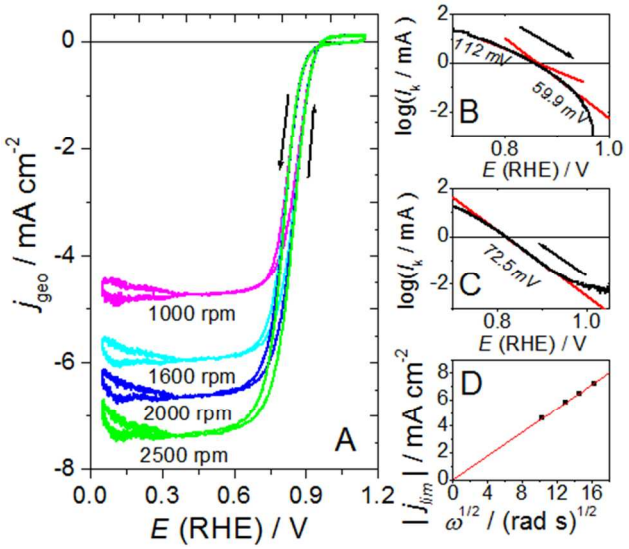

Figure 4: Polarization curves for the oxygen reduction at Pt(poly) in O_2-saturated 0.1 M $HClO_4$ at different rotation rates (A). Scan rate 0.1 V s^{-1}. Logarithm of I_k *vs.* E in the positive- (B) and negative-going directions (C), and the absolute value of j_{lim} *vs.* $\omega^{1/2}$ – Levich plot– (D).

In contrast, when v is large relative to ω, the time of the experiment is short and diffusion predominates over convection, $\delta_{diff} << \delta_{\omega}$ [56-62,87]. Under such a condition, *j-E* profiles for single electrochemical reactions at both, stationary and rotating disk electrodes, should have a current peak, j_p, proportional to $\sqrt{v}$, Eqn. (5), and independent of ω in the case of RDEs [56-62,87]. Conversely, ORR voltammograms at RDEs on Pt(poly) under this condition are characterized by a single and irreversible reduction peak, j_p^{ORR}, between 0.7 and 0.8 V, whose magnitude depends not only on v but also on ω, being greater at faster ω and constant v, Fig 3C.

An important detail in curves in Figs. 3A and 3B is the absence of peaks before, or after, j_p^{ORR}'s, even at fast scan rates that could suggest the existence of strong adsorption of reactants or intermediates, for which j_p would increase directly proportional to the v [31]. This fact would reveal a lack of adsorbed species during the ORR, additional to OH_{ads} and O_{ads} already present in the surface from water dissociation, Eqns. (-9) and (-10), as in O_2-free solutions [16,52,63,64,82,88], as reported by other studies [4,5,16,65,83]. In consequence, the coverage of ORR adsorbed intermediates coming from charge transfer steps different to Eqns. (9) and (10) for OH_{ads} and O_{ads} species, respectively, can be considered negligible [4,5,65].

$$PtOH_{ads} + H^+ + e^- \rightleftarrows PtH_2O_{ads} \qquad (9, -9)$$

$$PtO_{ads} + H^+ + e^- \rightleftarrows PtOH_{ads} \qquad (10, -10)$$

This result, however, does not imply that the amount of adsorbed O-containing species during the ORR would be the same as in O_2-free solutions, and it could be higher, as indicated by X-ray photoelectron spectroscopy (XPS) [11], electrochemical quartz crystal microbalance (EQCM) measurements [14,78], and studies at microelectrodes [54,55]. Concerted O_2-reduction/surface oxidation processes, as Eqn. (4), not directly involving a charge transfer could account for an increased coverage, as supported by recent theoretical calculations [79,80]. Besides, this result would also indicate that ORR intermediates could not be able to compete for Pt empty sites with OH_{ads} and O_{ads} species, because of either a weaker adsorption energy or serious mass transport limitations, *i.e.* low concentrations, $C <$

10^{-5} M [89]. As a result, inner-sphere reactions during the ORR may be promoted, rather than inhibited, by some adsorbed O-containing species [79,80], probably OH_{ads}.

An analysis of j_p^{ORR} as a function of v indicates that peak currents at stationary electrodes for continuous CVs are relatively constant with $\sqrt{\frac{n_a F v}{RT}}$, and lower in magnitude than expected for a $4e^-$ transfer reaction, indicating a control by a chemical reaction instead of a charge transfer, as clearly seen in Fig. 3C. However, j_p^{ORR} approaches the expected value for a $4e^-$ transfer when the electrode potential was first held at the OCP for a time long enough to reach $j_p^{ORR}{}_{lim}$ in Fig. 1 at 0.1 V s^{-1} (and at 0.05 V s^{-1}), as it is depicted by (ж) in Fig. 3C. This result indicates that if enough time is allowed at $E_i > E_{onset}^{ORR}$, current peaks at stationary electrodes and slow v´s could be described by Eqn. (5).

At RDEs, j_p^{ORR}'s are always higher relative to stationary electrodes, and the difference raises with ω, although not proportionally to $\sqrt{\frac{n_a F v}{RT}}$ in the whole range of v, except at small values, Fig. 3C. Initially j_{lim}´s are constant at increasing $\sqrt{\frac{n_a F v}{RT}}$, and with a magnitude equivalent to a charge transfer of ~3.8 (n_{eff}) under steady-state conditions, but once the diffusional control is reached, j_p^{ORR}'s grow with $\sqrt{\frac{n_a F v}{RT}}$ first with a slope close to the theoretical value for a reversible, but later for an irreversible, $4e^-$ transfer. At faster v's, j_p^{ORR}'s now rise with $\sqrt{\frac{n_a F v}{RT}}$ at a smaller slope than the one expected for a $1e^-$ transfer, and later become independent of v. This transition depends on ω and takes place at 0.5 and 10 V s^{-1} at 70 and 2500 rpm, respectively.

Results in Fig. 3 illustrate a dual reaction dynamics during the ORR on platinum surfaces depending on the value of the scan rate relative to the rotation rate, and confirms the presence of at least one chemical step in the mechanism [31,37,41-51]. At slow v, and if enough time is given at $E_i > E_{onset}^{ORR}$ on stationary electrodes, the system behaves like an almost $4e^-$ transfer process, while at faster scan rates, the sweep is finished before the chemical reaction can occur at full extent, and reduction currents become even lower than the ones expected for a $1e^-$ transfer reaction.

Moreover, differences in j_p^{ORR}'s at different ω but constant v, as in Fig. 3A and 3B, can only be explained by considering the existence of, at least, two soluble species with different diffusion coefficients. Different studies have shown larger currents than expected in LSVs owing to the coupling of the diffusional pathways by very fast reactions of species in the diffusion layer with different diffusion coefficients, as in the case of homogeneously catalyzed reactions [90-93]. In our case, the thickness of the diffusion layer of one of the species is being determined by ω, Eqn. (6), while the other one by v. Then, changing ω at constant v would modify the flux of the soluble species whose diffusion layer is controlled by ω, giving rise to changes in j_p^{ORR} [13,16,34]. If only one soluble species were present, or several ones with equal D, identical j_p^{ORR}'s would have been observed at constant v, regardless of ω [31], since the concentration profiles close to the surface are only controlled by the magnitude of D, [56-61,87].

In order to validate this interpretation of experimental data, five simple electrochemical reaction schemes were simulated. *i*) A simple multi-electron transfer. *ii*) A chemical reaction preceding a multi-electron transfers: a *CE*-mechanism [41,42]. *iii*) A chemical reaction following a multi-electron transfers: an *EC*-mechanism [42]. *iv*) A first-order chemical reaction between two single charge transfers with $E_1° < E_2°$ (only one peak in the LSV): an *ECE*-mechanism [43-48,49-51]. *v*) An EC-mechanism followed by a second-order disproportionation reaction of the final product to partially regenerate the initial reactant, in which the chemical reaction is the RDS: the so-called *DISP1*-mechanism [38,44-48,50,51,69-71]. In all cases, reaction schemes at different rotation rates were evaluated by assuming fast and/or slow charge transfers (α = 0.5), reversible and/or irreversible chemical reactions, and different diffusion coefficients for reactants, $D_{reactant}$, and products, $D_{product}$. The complexity of the ORR precludes a full simulation of the, still unknown, whole reaction mechanism and only a semi-qualitative approach was attempted to understand the strong effect of ω on j_p^{ORR}'s at constant v shown in Fig. 3.

Figure S4 resumes representative LSVs for each of one the simulated mechanisms under relevant parameters. A detailed description of these current responses is out of the scope of this work and will be discussed elsewhere. Regarding the present study, simulated curves evidenced that only a fast surface chemical reaction producing a soluble species preceding

the initial charge transfer, a $C_s^{fast}E$-mechanism, Eqns. (11), with $D_{reactant} \neq D_{product}$, could give rise to differences in j_p in LSVs at different rotation rates under diffusional control, Fig. S4C. In this case, if $D_{reactant} < D_{product}$, j_p´s decreases with ω, but if $D_{reactant} > D_{product}$, j_p´s increases with ω, as experimentally occurs. For $D_{reactant} = D_{product}$, j_p´s at stationary electrodes and RDEs at transient conditions superpose and follow a similar dynamics as in the case of single electron transfers, Eqn. (5) [37,46,50,56-59,61,87].

$$Z + M \overset{K}{\Leftrightarrow} M - A_{ads} \qquad (11a)$$

$$M - A_{ads} \overset{K}{\Leftrightarrow} M + A \qquad (11b)$$

$$A + 1e^- \rightleftarrows B \qquad (11c)$$

For the other reaction schemes changes in j_p with v are not affected by ω, and j_p´s at stationary electrodes and RDEs under non-steady state conditions superimpose and follow Eqn. (5). This can be appreciated in simulated curves in Fig. S4 for simple multi-electron transfers, Fig. S4A, tan *EC*-mechanism, Fig. S4D, an *ECE*-mechanism with $E_1° < E_2°$, Fig. S4E, and a *DISP*-mechanism, Fig. S4F. Thus, any of these mechanistic schemes cannot account for the effect of ω on j_p^{ORR}´s at constant v in Fig. 3.

As a matter of example, Figure 5 resumes simulated LSV scans at ω = 70 and 2500 rpm and several scan rates for an irreversible, and fast, surface chemical reaction of a soluble reactant producing a soluble species, $k = 1x10^5$ M^{-1} s^{-1}, preceding a four-electron transfer with a slow first charge transfer, Eqns. (11). Additionally, graphs of normalized j_p as a function of the normalized square root of the scan rate, as in Fig. 3C, are also given in Fig. 5C, including the expected tendency at stationary electrodes. For calculations, system parameters, $D_z = D_{O_2} = 1.93x10^{-5}$ cm^2 s, $C^0_{O_2}$ and υ, were those given in previous paragraphs for the ORR in 0.1 M $HClO_4$, $D_A = D_B = 1.0x10^{-5}$ cm^2 s, and the concentration of surface active sites was assumed constant. Similar curves were also calculated for a reversible surface chemical reaction, as long as the equilibrium reaction constant is high enough, $K > 1x10^4$ M^{-1} m^2, and regardless of the magnitude of the forward or backward reaction rates. For lower values of K, peak currents for curves at 70 and 2500 rpm superimpose, as it can be appreciated in Fig. S4B.

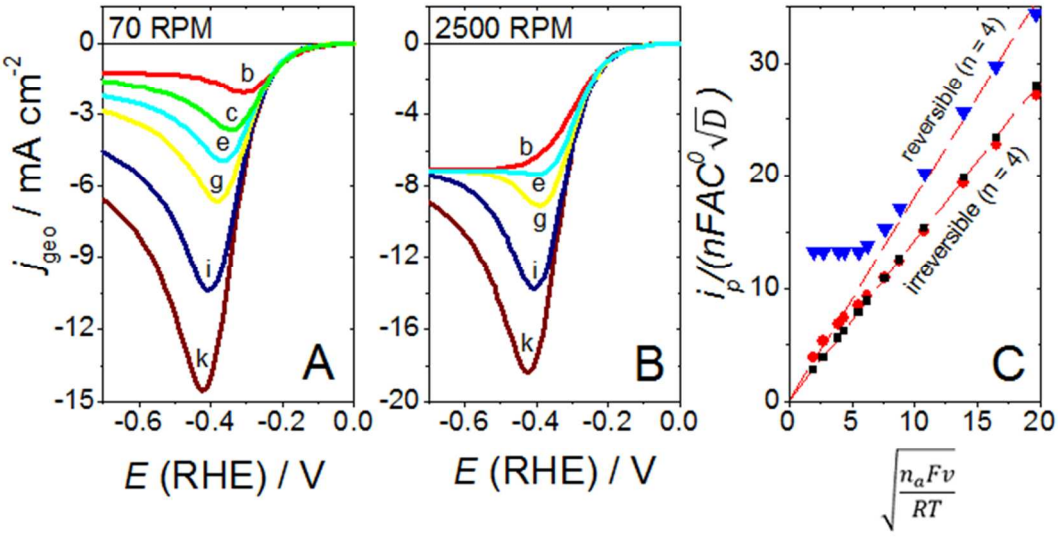

Figure 5: Simulated negative-going scans at (A) 70 and (B) 2500 rpm for an irreversible surface chemical reaction producing a soluble species, $k = 1x10^5$ M^{-1} s^{-1}, preceding a 4-electron transfer with a slow first charge transfer. Scan rates are: b) 0.1; c) 0.4; e) 1.0; g) 2.0; i) 5.0; k) 10 V s^{-1}. (C) Normalized peak currents against the square root of the normalized scan rate at stationary (■), and rotating disk electrodes: 70 (●) and 2500 rpm (▼). For the sake of comparison, theoretical curves for single four, $n = 4$, total charge transfers with a first fast and slow ($\alpha = 0.5$) electron transfer are also given (dashed lines).

In simulations in Fig. 5, the value of D_A, representing the intermediate species, was chosen to be in-between the values for D_{O_2} and $D_{H_2O_2} = 0.87x10^{-5}$ cm^2 s [94] in 0.1 M $HClO_4$, as expected for species of similar masses that differ only in the magnitude of the charge and/or the number of hydrogen bounds with the solvent [93,95]. In agreement, reported diffusion coefficients for the superoxide ion, O_2^-, in alkaline aqueous solutions and dimethyl sulfoxide are 1.07 [95], and 3.00 [96], times smaller than for O_2, respectively, but greater than for H_2O_2. A smaller D indicates a higher solvation of the species or the formation of ion pairs and/or hydrogen bonds with the supporting electrolyte [96]. Nevertheless, close to the electrode it is probable that all these species experience effective diffusion coefficients smaller than on the bulk, owing to interactions with the surface.

As it is seen in Fig. 5, all LSV's under diffusional control have larger values of j_p´s at 2500 than at 70 rpm. This difference appears because the thickness of the diffusional layer

of the reactant, δ_{diff}^{Z}, in the initial fast chemical reaction, Eqn. (11a), is controlled by ω at RDEs, $\delta_{diff}^{Z} = \delta_{\omega}^{Z}$, and $D_z > D_A$. Then, at faster ω the flux of Z toward the surface increases, where it is transformed into A, which diffuses back into the body of the solution at a slower rate than the rate at which Z is arriving to the surface, causing an increase in the concentration of A close to the electrode. Under these conditions, j_p´s would depend on ω, as it is shown in Fig. 5C.

In contrast, when convection predominates over diffusion, $\delta_{diff} = \delta_{\omega}$ for both Z and A, and this latter cannot accumulate close to the surface. In this case, typical sigmoidal, S-shaped curves of steady-state RDEs are measured (slow v), curves *b* and *e* at 2500 rpm in Fig. 5B. Eventually, though, v would be fast enough relative to the reaction rate of the initial chemical step to forbid a substantial accumulation of A, and j_p´s would follow Eqn. (5) regardless of ω, as it is seen for $\sqrt{\frac{n_a F v}{RT}} > 10$, $v > 1.0$ V s^{-1}, at 70 rpm in Fig. 5C.

Worth mentioning, that the dynamics just described in Fig. 5 only can be evidenced by comparing LSVs under transient conditions at different v´s at stationary electrodes and RDEs. Only in this way, it is possible independently to control the mass transport of the reactant, Z, and the intermediate species, A, by properly adjusting ω and v, respectively. In contrast, if microelectrodes were employed, it would not be possible to measure this effect under the same set up, and microelectrodes of different sizes would be necessary to reproduce the effect of changing ω. This is because the transition between spherical and planar diffusion in microelectrodes can only be controlled by changing v or the diameter of the microelectrode, and only measurements under planar diffusion conditions are equivalent to those ones at RDEs at a δ_{ω} equivalent to the electrode diameter [31].

Note also that, although the presence of an initial fast chemical step before the first charge transfer in the ORR mechanism at Pt surfaces has been suggested since early works [1,5,6,17-19], and by recent theoretical studies [79,80], results presented here provide experimental evidence for its existence. This fact, together with the formation of a soluble species before the first charge transfer also implies that at potentials close to the reaction onset the dissociative adsorption of oxygen is not the preferential reaction path for the ORR in these surfaces, as it is rather improbable that O_{ads} could go to the solution before undergoing an electron transfer. This situation could change of course at lower potentials,

because of the decrease in the surface coverage of O-containing species, but no experimental evidence of this change has been given so far.

A clear difference between curves in Figs. 3C and 5C is the leveling in j_p^{ORR}'s at increasing scan rates. As discussed in the introduction, this feature clearly indicates that the current is controlled by a chemical reaction instead of a charge transfer at those scan rates at which curves deviate from the expected tendency, as in the case of the *ECE*- and *DISP*-mechanism in Fig. S4. Hence, while differences in j_p's between curves at 70 and 2500 rpm can be only explained by an initial and fast chemical reaction, the presence of a current plateau in Fig. 3C anticipates the presence of another chemical step between two charge transfers inside the ORR mechanism on Pt surfaces. The possible occurrence of this second chemical reaction will be analyzed in detail in the future.

3.3. First steps in the ORR mechanism on Pt surfaces

As it has been shown, O_2 reacts with the surface at potentials close to the reaction onset to produce a soluble species before the first electron transfer takes place. Unfortunately, from electrochemical results alone, it is not possible undoubtedly to identify neither the real ORR path nor the chemical nature of the soluble intermediate, and data from other available experimental techniques under similar conditions have not reported its possible existence so far. This fact could be because either the physical or chemical properties of the intermediate cannot be measured with current methods or equipments are not sensitive enough to detect it. Nevertheless, all the information given above provides new ORR mechanistic insights that certainly help to discard some proposed routes, as the initial dissociative adsorption of oxygen, and possibly will open new horizons toward the molecular understanding of this important reaction. In what follows, an analysis of available theoretical and experimental results will be performed to suggest possible first steps in the ORR mechanism in light of results discussed above.

From early studies at Pt(poly), it is known that an steady OCP in O_2-saturated solutions is slowly established, and follows a first order dependence on C^0_{O2}, albeit no increase in j_p^{ORR}, as in Fig. 1, was reported before. It has been proposed that the nature of this OCP could be either a Nernst potential controlled by $O_2/HO_2^*{}_{ads}$ and O_2/H_2O_2 couples, depending

on the solution pH [68], or a mixed potential between Eqn. (1) and an unknown oxidation reaction. Pt surface oxidation, Eqns. (-9) and (-10), [66,67], oxidation of residual impurities [65] or even Pt dissolution [18] had been proposed to be the anodic part of this mixed potential. However, none of these alternatives appears to be able to support the experimental corrosion current density of ~10^{-7} A cm^{-2}, which would require a concentration of ~10^{-6} M for the participating species [18,66,67].

On the other hand, an spectroscopic study in alkaline solutions identified adsorbed superoxide ion, $O_{2,ads}^-$, as an intermediate in the ORR on Pt(poly) [75], giving support to the $O_2/O_{2,ads}^-$ couple as responsible of the OCP value. Likewise, infrared spectroscopic studies at the Pt/Nafion interface under O_2 atmosphere reported an adsorbed ORR intermediate in acid environments [76], first ascribed to adsorbed oxygen, $O_{2,ads}$, [76], but later to $O_{2,ads}^-$ [14]. Hence, both soluble O_2^- and/or hydroperoxyl, HO_2^*, radicals could be in principle the species responsible of results in Figs. 1 and 2. Nonetheless, because of the protonation equilibrium of the O_2^-/HO_2^* couple, Eqn. (12), pKa = 4.8, the HO_2^* radical is the most favored species in acid media [95,97,98]. Though, $O_{2\,ads}^-$ could be still initially formed on the surface, given the influence of the surface on the pKa of adsorbates and soluble species in the proximity of the electrode [99,100].

$$O_2^- + H^+ \rightleftarrows HO_2^* \qquad (12)$$

In contrast, OH^* radicals, although reported to appear during the ORR at Pt(poly) [101], and suspected to occur during the reduction/oxidation of H_2O_2 [101-103], cannot explain results in Figs. 1 and 2 mainly for three reasons. First, j_p^{ORR} after longer τ_h, curve *i* in Fig. 1, approaches a limiting value, $j_p^{ORR}{}_{lim}$, equivalent to the expected value for a transfer of $4e^-$ (see Fig. 3C), implying that the soluble species is in equilibrium with surface species, while the production of OH^* radicals is expected to be quite irreversible. Second, OH^* radicals are expected to be highly reactive and thus, reduction currents would be expected if they are produced at $E_i > E_{onset}^{ORR}$. Third, OH^* radicals typically react at reaction rates near to the diffusion controlled limit [97,104], making somewhat unlikely its accumulation to reach detection levels as in Figs. 1, 2 and S2. Contrarily, soluble O_2^- and HO_2^* radicals are less mobile and reactive than OH^*.

Under this general scenario, the production of HO_2^*, or O_2^- followed by fast protonation [99], can be proposed to be the first step in the ORR mechanism: Eqn. (4) coupled to Eqn. (9). This last equation could be both the potential determining step [99], and the RDS, as commonly suggested. The change in Tafel slopes during the ORR could be then explained owing to the decrease in the adsorption energy for this step, $\Delta G_0^{OH_{ads}/H_2O_{ads}}$, at high $H_2O_{ads}/OH_{ads}/O_{ads}$ coverages, Table S1, as suggested by both experimental and theoretical studies [12,15,16,52,63,64,77,88]. At decreasing potentials, $\Delta G_0^{OH_{ads}/H_2O_{ads}}$ would increase, due to the decrease in the O-containing coverage at the surface, which in turn would promote the reaction.

The natural question is then why if HO_2^* radicals can be produced and accumulated at potentials higher than E_{onset}^{ORR}, no reduction currents are measured at those potentials. This remains an open question, but the most probable reason for this fact is the existence competing reactions at those potentials. In this sense, it is known that both O_2^- and HO_2^* radicals undergo fast and interrelated, second order, disproportionation reactions, Eqns. (13) and (14), to produce O_2 and H_2O_2 [95,97,98,105],

$$2HO_2^* \rightleftarrows H_2O_2 + O_2 \qquad (13)$$

$$O_2^- + HO_2^* \rightleftarrows HO_2^- + O_2 \qquad (14)$$

this last equation would be followed by fast protonation in acid solutions, Eqn. (15), due to the high pK_a of the protonation equilibrium between the HO_2^-/H_2O_2 couple in solution (pK_a = 11.6, Table S1),

$$HO_2^- + H^+ \rightleftarrows H_2O_2 \qquad (15)$$

At higher potentials produced H_2O_2, either by reaction Eqn. (13) or a subsequent reduction of HO_2^*, as in Eqn. (16), would oxidize back to O_2, Eqn. (-2), in a zero-current-cycle. The existence of such a zero-current-cycle at $E_i > E_{onset}^{ORR}$ during the ORR on Pt(poly) was first considered by Gerischer and Gerischer in 1956 [106], and it was recently invoked to explain the reaction over Pt(111) in acid environments [12,13,15,16].

$$HO_2^* + H^+ + e^- \rightleftarrows H_2O_2 \qquad (16)$$

Therefore, the rise in j_p^{ORR} in Figs. 1 and 2 would occur as soon as either the reduction of H_2O_2 or the rupture of the O-O bond of O_2^-/HO_2^* is allowed at $E_i \leq E_{onset}^{ORR}$ due to a double effect. First, the accumulation of HO_2^* in a thin reaction layer close to the surface, and

second the parallel regeneration of O_2 in the O_2-diffusion layer mainly by Eqn. (13). The high reactivity of the HO_2^* radical thanks to the disproportionation reaction would forbid the build-up of a high concentration of this species [44-51,99], for which an expected half-life in solution of $\tau_{½} > 1x10^{-3}$ s is estimated for concentrations lower than $\sim 1x10^{-3}$ M [95,97,99,104,105]. This last value is the bulk concentration of O_2 in the electrolyte that approximately gives the order of magnitude for the upper limit of the concentration of any of these two radicals that can be reached, considering the reaction rate for Eqn. (13), Table S1, and the lifetime for species undergoing second order reactions [31].

If HO_2^* is formed, its disproportionation, Eqn. (13), would act as a competing reaction for HO_2^* radicals during the ORR and thus, H_2O_2 would always be formed, whether or not its formation also takes place inside the main mechanism. This possibility would explain the production of H_2O_2 as a direct consequence of the reduction of oxygen on Pt surfaces, as suggested by studies in nanostructured Pt electrodes [8-10,25-30], and not because of impurities in the solution, but its detection does not undoubtedly imply an operative serial mechanism, as usually believed. Moreover, regardless of the exact mechanism, the fact that HO_2^* radical and H_2O_2 would be always produced during the ORR on Pt would profoundly affect the durability of Pt-based materials employed in fuel cell and should be taken into account in the design of new composites for fuel cell cathodes.

Notice that although adsorbed $HO_2^*{}_{ads}$ was proposed to be the most probable ORR intermediate in past studies [5,6,17-22,75], results in this work would be a first indirect electrochemical evidence of both its existence as intermediate and the presence of a zero current cycle at $E_i \geq E_{onset}^{ORR}$. Interestingly, the steady state potential for the O_2^-/HO_2^* radical couple in acid media is a mixed potential ca. ~1.05 V, at concentrations of ~ 1 to 50 μM [99]. These values are close to the OCP value in O_2-saturated, solutions at Pt(poly) electrodes, and the estimated concentration range necessary to explain the $\sim 10^{-7}$ A cm^{-2} corrosion current [18,65,66-68], which would indirectly support what it has been discussed here. Similarly, the reported value of the theoretical activation energy for the electrochemical reduction of HO_2^* to H_2O_2 [107,108], Eqn. (16), is also similar to experimental activation energies reported for the ORR on Pt basal planes and Pt(poly) in

both acid and alkaline solutions [7,19], and even on bimetallic surfaces of Pt_3-Ni and Pt_3Co [7].

The direct identification of HO_2^* as ORR intermediate, though, would be a more elusive subject than in the case of $O_{2,ads}^-$, that would explain why it has not been explicitly considered before. This is because HO_2^* is expected to be more reactive, and with a shorter lifetime, than O_2^- [95,97,104], and it is considered to be a better oxidizing than reducing agent [97,99]. So, even indirect electrochemical techniques such as RRDEs and SECM, or even double-step (or double scan) methods, known to be more powerful to characterize complex reaction than conventional dc procedures [48,50,51,109], could either fail to identify it or underestimate its production. Since currents from its heterogeneous reduction, Eqn. (16), would be masked by the parallel oxidation of the H_2O_2, Eqn. (-2), formed after disproportionation of HO_2^*, Eqn. (13). Together with the possibility of a surface catalyzed HO_2^* decomposition [99,102], Eqns. (-10), (17) and (18) or Eqns. (19) and (20), as reported for H_2O_2 [69-71,102], Eqns. (-9), (-19) and (21). The possibility of the parallel occurrence of all these reactions and the existence of adsorbed and soluble species clearly reflect the complexities of the ORR mechanism.

$$PtOH_{ads} + HO_2^* \rightleftarrows PtO_{ads} + H_2O_2 \qquad (17)$$

$$PtO_{ads} + HO_2^* \rightleftarrows PtOH_{ads} + O_2 \qquad (18)$$

$$H_2O + PtHO_{2,ads}^* \rightleftarrows PtOH_{ads} + H_2O_2 \qquad (19, -19)$$

$$PtOH_{ads} + HO_2^* \rightleftarrows +PtH_2O_{ads} + O_2 \qquad (20)$$

$$PtHO_{2,ads}^* + H_2O_2 \rightleftarrows O_2 + H_2O + PtOH_{ads} \qquad (21)$$

Before finishing, it is important to highlight that the suggestion of HO_2^* as the possible ORR soluble intermediate is rather circumstantial, and additional experiments are required to confirm or reject this option. In principle, any other species able to explain described experimental results would be a possible intermediate. For example, it can be also proposed that singlet oxygen species, $^1O_2$, or soluble platinum forms could be the soluble intermediate. However, after a fast analysis, HO_2^* was considered as the more suitable candidate, although at this stage the other options cannot be completely ruled out. In the case of $^1O_2$, studies with Pt NPs have shown a highly *pH*-dependent scavenging activity toward $^1O_2$, being more active at high *pH*s [102]. Thus, if $^1O_2$ were the soluble species, a

lower catalytic activity were expected at increasing *pH*. However, ORR studies at different *pH*s have shown a decrease in limiting currents at $2.8 < pH < 5.6$, but similar ORR activities at $pH = 1$ and 13 [33], which would not be expected from an increasing $^1O_2$ scavenging activity with the *pH*.

Similarly, the Pt dissolution process in O_2-saturated environments is a slow process that gives rise to equilibrium concentrations of soluble Pt species around ~ 6 μM after long times (> 50 h) [110,111]. In contrast, results in Figs. 1 to 3 took only few seconds to be recorded and hence, the expected amount of soluble Pt species is practically negligible. Note that ~150 s at the OCP were required for a four-times increase in the transferred charge, as it is seen in Fig. 1B. Furthermore, theoretical studies for competing homogeneous and heterogeneous catalytic reactions have estimated that the homogeneous pathway becomes unimportant relative to the heterogeneous one at small [catalyst]/[reactant] ratios [92]. Thus, even if soluble Pt forms are active catalysts for the ORR, their participation in above results is expected to be negligible. Nevertheless, it is highly probable that surface Pt oxides participate as redox couples during the ORR, as discussed in the text and analogous to certain macrocyclic metal complexes [112].

4. Conclusions

In this work, a detailed study of the oxygen reduction reaction on platinum surfaces has been presented under non-steady state conditions. Results reveal the presence of kinetic effects inside the ORR mechanism, demonstrating the occurrence of an initial chemical reaction before the first charge transfer and the production of a soluble intermediate species during the reaction. In addition, results support the fact that dissolved oxygen reacts at potentials higher than the reaction onset, although no reduction currents are measured, and that this process controls the value of peak currents at lower potentials. Finally, possible reaction mechanisms are discussed in which both the disproportionation of the hydroperoxyl radical and the formation of hydrogen peroxide at high potentials are main

reasons for the lack of reduction current at potentials higher than the experimentally measured reaction onset potential.

Associated content

Supporting information: Additional supporting electrochemical characterization, calculated LSV curves for simple reaction schemes by numerical simulation and estimated thermodynamic and kinetic parameters for the reaction steps discussed in the text.

Acknowledgments

The authors would like to thank Fundação de Amparo a Pesquisa do Estado de São Paulo (FAPESP - Procs. 2013/16930-7 and 2014/23486-9), Brazil (A.M.G-M. and E.A.T.) and the Spanish MINECO through project CTQ2016-76221-P (FEDER) and GV through PROMETEOII/2014/013 (FEDER) (J.M.F.), for financial supports.

References

1. Kinoshita, K. Electrochemical Oxygen Technology; John Wiley and Sons: New York, 1992.
2. Stamenkovic, V.R.; Fowler, B.; Mun, B.S.; Wang, G.; Ross, P.N.; Lucas, C.A.; Markovic, N.M. Improved Oxygen Reduction Activity on $Pt_3Ni(111)$ via Increased Surface Site Availability. *Science* **2007**, *315*, 493-497.
3. Snyder, J.; Fujita, T.; Chen, M.W.; Erlebacher, J. Oxygen Reduction in Nanoporous Metal–Ionic Liquid Composite Electrocatalysts. *Nature Mater.* **2010**, *9*, 904-907.
4. Breiter, M.W. Voltammetric Study of the Reduction of Molecular Oxygen on Bright Platinum in Perchloric Acid Solution. *Electrochim. Acta* **1964**, *9*, 441-450.
5. Damjanovic, A.; Brusic, V. Electrode Kinetics of Oxygen Reduction on Oxide–Free Platinum Electrodes. *Electrochim. Acta* **1967**, *12*, 615-628.
6. Paucirova, M.; Drazic, D.M.; Damjanovic, A. The Effect of Surface Coverage by Adsorbed Oxygen on the Kinetics of Oxygen Reduction at Oxide Free Platinum. *Electrochim. Acta* **1973**, *18*, 945-951.

7. Markovic, N.M.; Ross, P.N., Jr. Surface Science Studies of Model Fuel Cell Electrocatalysts. *Surf. Sci. Rep.* **2002**, *45*, 117-229.
8. Kabbabi, A.; Gloaguen, F.; Andolfatto, F.; Durand, R. Particle Size Effect for Oxygen Reduction and Methanol Oxidation on Pt/C inside a Proton Exchange Membrane. *J. Electroanal. Chem.* **1994**, *373*, 251-254.
9. Antoine, O.; Bultel, Y.; Durand, R.; Ozil, O. Electrocatalysis, Diffusion and Ohmic Drop in PEMFC: Particle Size and Spatial Discrete Distribution Effects. *Electrochim. Acta* **1998**, *43*, 3681-3691.
10. Antoine, O.; Bultel, Y.; Durand, R. Oxygen Reduction Reaction Kinetics and Mechanism on Platinum Nanoparticles Inside Nafion®. *J. Electroanal. Chem.* **2001**, *499*, 85-94.
11. Wakisaka, M.; Suzuki, H.; Mitsui, S.; Uchida, H.; Watanabe, M. Increased Oxygen Coverage at Pt−Fe Alloy Cathode for the Enhanced Oxygen Reduction Reaction Studied by EC−XPS. *J. Phys. Chem. C* **2008**, *112*, 2750-2755.
12. Gómez-Marín, A.M.; Rizo, R.; Feliu, J.M. Some Reflections on the Understanding of the Oxygen Reduction Reaction at Pt(111). *Beilstein J. Nanotechnol.* **2013**, *4*, 956-967.
13. Gómez-Marín, A.M.; Feliu, J.M. New Insights into the Oxygen Reduction Reaction Mechanism on Pt (111): A Detailed Electrochemical Study. *ChemSusChem.* **2013**, *6*, 1091-1100.
14. Omura, J.; Yano, H.; Tryk, D.A.; Watanabe, M.; Uchida, H. Electrochemical Quartz Crystal Microbalance Analysis of the Oxygen Reduction Reaction on Pt-based Electrodes. Part 2: Adsorption of Oxygen Species and ClO_4^- Anions on Pt and Pt−Co Alloy in $HClO_4$ Solutions. *Langmuir* **2014**, *30*, 432-439.
15. Gómez-Marín, A.M.; Rizo, R.; Feliu, J.M. Oxygen Reduction Reaction at Pt Single Crystals: A Critical Overview. *Catal. Sci. Technol.* **2014**, *4*, 1685-1698.
16. Gómez-Marín, A.M.; Feliu, J.M. Role Of Oxygen-Containing Species at Pt(111) on the Oxygen Reduction Reaction in Acid Media. *J. Solid State Electrochem.* **2015**, *19*, 2831-2841.

17. Damjanovic, A.; Genshaw, A. Dependence of the Kinetics of O_2 Dissolution at Pt on the Conditions for Adsorption of Reaction Intermediates. *Electrochim. Acta* **1970**, *15*, 1281-1283.
18. Sepa, D.B.; Vojnovic, M.V.; Damjanovic, A. Reaction Intermediates as a Controlling Factor in the Kinetics and Mechanism of Oxygen Reduction at Platinum Electrodes. *Electrochim. Acta* **1981**, *26*, 781-793.
19. Sepa, D.B.; Vojnovic, M.V.; Vracar, L.M.; Damjanovic, A. Apparent Enthalpies of Activation of Electrodic Oxygen Reduction at Platinum in Different Current Density Regions I. Acid Solution. *Electrochim. Acta* **1986**, *31*, 91-96.
20. Damjanovic, A.; Genshaw, M.A.; Bockris, J.O. The Role of Hydrogen Peroxide in the Reduction of Oxygen at Platinum Electrodes. *J. Phys. Chem.* **1966**, *70*, 3761-3762.
21. Damjanovic, A.; Genshaw, M.A.; Bockris, J.O. The Role of Hydrogen Peroxide in Oxygen Reduction at Platinum in H_2SO_4 Solution. *J. Electrochem. Soc.* **1967**, *114*, 466-472.
22. Damjanovic, A.; Genshaw, M.A.; Bockris, J.O. The Mechanism of Oxygen Reduction at Platinum in Alkaline Solutions with Special Reference to H_2O_2. *J. Electrochem. Soc.* **1967**, *114*, 1107-1112.
23. Wroblowa, H.S.; Pan, Y.-C.; Razumney, G. Electroreduction of Oxygen: A New Mechanistic Criterion. *J. Electroanal. Chem. Interfacial Electrochem.* **1976**, *69*, 195-201.
24. Fischer, P.; Heitbaum, J. Mechanistic Aspects of Cathodic Oxygen Reduction. *J. Electroanal. Chem.* **1980**, *112*, 231-238.
25. Watanabe, M.; Sei, H.; Stonehart, P. The Influence of Platinum Crystallite Size on the Electroreduction of Oxygen. *J. Electroanal. Chem.* **1989**, *261*, 375-387.
26. Inaba, M.; Yamada, H.; Tokunaga, J.; Tasaka, A. Effect of Agglomeration of Pt/C Catalyst on Hydrogen Peroxide Formation. *Electrochem. Solid-State Lett.* **2004**, *7*, A474-A476.
27. Chen, S.; Kucernak, A. Electrocatalysis under Conditions of High Mass Transport Rate: Oxygen Reduction on Single Submicrometer-Sized Pt Particles Supported on Carbon. *J. Phys. Chem. B* **2004**, *108*, 3262-3276.

28. Seidel, Y.E.; Schneider, A.; Jusys, Z.; Wickman, B.; Kasemo, B.; Behm, R.J. Mesoscopic Mass Transport Effects in Electrocatalytic Processes. *Faraday Discuss.* **2008**, *140*, 167-184.
29. Schneider, A.; Colmenares, L.; Seidel, Y.E.; Jusys, Z.; Wickman, B.; Kasemo, B.; Behm, R.J. Transport Effects in the Oxygen Reduction Reaction on Nanostructured, Planar Glassy Carbon Supported Pt/GC Model Electrodes. *Phys. Chem. Chem. Phys.* **2008**, *10*, 1931-1943.
30. Gara, M.; Laborda, E.; Holdway, P.; Crossley, A.; Jones, C.J.V.; Compton, R.G. Oxygen Reduction at Sparse Arrays of Platinum Nanoparticles in Aqueous Acid: Hydrogen Peroxide as a Liberated Two-Electron Intermediate. *Phys. Chem. Chem. Phys.* **2013**, *15*, 19487-19495.
31. Bard, A.J.; Faulkner, L. R. Electrochemical Methods: Fundamentals and Applications, 2nd ed.; John Wiley and Sons: New York, 2001.
32. Scherson, D.A.; Tolmachev, Y.V. Impurity Effects on Oxygen Reduction Electrocatalysis at Platinum Ultramicroelectrodes: A Critical Assessment. *Electrochem. Solid-State Lett.* **2010**, *13*, F1-F2.
33. Briega-Martos, V.; Herrero, E.; Feliu J.M. Effect of pH and Water Structure on the Oxygen Reduction Reaction on Platinum Electrodes. *Electrochim. Acta* **2017**, *241*, 497-509.
34. Gómez-Marín, A.M.; Feliu, J.M. Oxygen Reduction on Platinum Single Crystal Electrodes, Reference Module in Chemistry, Molecular Sciences and Chemical Engineering. https://doi.org/10.1016/B978-0-12-409547-2.13333-5, 2017.
35. Malachesky, P.A.; Marcoux, L.S.; Adams, R.N. Homogeneous Chemical Kinetics with the Rotating Disk Electrode. *J. Phys. Chem.* **1966**, *70*, 4068-4070.
36. Karp, S. Homogeneous Chemical Kinetics with the Rotating Disk Electrode. The ECE Mechanism. *J. Phys. Chem.* **1968**, *72*, 1082.
37. Nadjo, L.; Savéant, J.-M. Electrodimerization VIII. Role of Proton Transfer Reactions in the Mechanism of Electrohydrodimerization Formal Kinetics for Voltammetric Studies (Linear Sweep, Rotating Disc, Polarography). *J. Electroanal. Chem.* **1973**, *44*, 327-366.

38. Compton, R.G.; Harland, R.G.; Unwin, P.R.; Waller, A.M. Rotating-Disc Electrodes ECE and DISPl Processes. *J. Chem. Soc. Faraday Trans. 1* **1987**, *83*, 1261-1268.
39. Compton, R.G.; Unwin, P.R. Rotating-Disc Electrode Voltammetry. Digital Simulation of the Current-Voltage Behaviour of Electrode Processes Involving Reversible Electron-Transfer and Coupled Homogeneous Kinetics. *J. Chem. Soc. Faraday Trans. 1* **1989**, *85*, 1821-1834.
40. Pletcher, D.; Sotiropoulos, S. A Study of Cathodic Oxygen Reduction at Platinum Using Microelectrodes. *J. Electroanal. Chem.* **1993**, *356*, 109-119.
41. Savéant, J.-M.; Vianello, E. Potential-Sweep Chronoamperometry Theory of Kinetic Currents in the Case of a First Order Chemical Reaction Preceding the Electron-Transfer Process. *Electrochim. Acta* **1963**, *8*, 905-923.
42. Nicholson, R.S.; Shain, I. Theory of Stationary Electrode Polarography Single Scan and Cyclic Methods Applied to Reversible, Irreversible, and Kinetic Systems. *Anal. Chem.* **1964**, *36*, 706-723.
43. Nicholson, R.S.; Shain, I. Experimental Verification of an ECE Mechanism for the Reduction of p-Nitrosophenol, using Stationary Electrode Polarography. *Anal. Chem.* **1965**, *37*, 190-195.
44. Mastragostino, M.; Savéant, J.-M. Disproportionation and ECE Mechanisms-II. Reduction of the Uranyl Cation in Perchloric Acid. *Electrochim. Acta* **1968**, *13*, 751-762.
45. Nadjo, L.; Savéant, J.-M. Linear Sweep Voltammetry: Kinetic Control by Charge Transfer and/or Secondary Chemical Reactions I. Formal Kinetics. *J. Electroanal. Chem.* **1973**, 48, 113-145.
46. Amatore, C.; J.-M. Savéant, ECE and Disproportionation. Part V. Stationary State General Solution Application to Linear Sweep Voltammetry. *J. Electroanal. Chem.* **1977**, *85*, 27-46.
47. Mastragostino, M.; Nadjo, L.; Savéant, J.-M. Disproportionation and ECE Mechanisms-I. Theoretical Analysis. Relationships for Linear Sweep Voltammetry. *Electrochim. Acta* **1968**, *13*, 721-749.

48. Andrieux, C.P.; Nadjo, L.; Savéant, J.-M. Electrodimerization I. One-Electron Irreversible Dimerization. Diagnostic Criteria and Rate Determination Procedures for Voltammetric Studies. *J. Electroanal. Chem.* **1970**, *26*, 147-186.
49. Nicholson, R.S.; Shain, I. Theory of Stationary Electrode Polarography for a Chemical Reaction Coupled Between Two Charge Transfers. *Anal. Chem.* **1965**, *37*, 178-190.
50. Amatore, C.; Savéant, J.-M. Do ECE Mechanisms Occur in Conditions Where They Could Be Characterized by Electrochemical Kinetic Techniques? *J. Electroanal. Chem.* **1978**, *86*, 227-232.
51. Amatore, C.; Savéant, J.-M. ECE and Disproportionation Part VI. General Resolution. Application to Potential Step Chronoamperometry. *J. Electroanal. Chem.* **1979**, *102*, 21-40.
52. Angerstein–Kozlowska, H.; Conway, B.E.; Sharp, W.B.A. The Real Condition of Electrochemically Oxidized Platinum Surfaces. Part I. Resolution of Component Processes. *J. Electroanal. Chem. Interfacial Electrochem.* **1973**, *43*, 9-36.
53. Chen, Q.-S.; Solla-Gullón, J.; Sun, S.-G.; Feliu, J.M. The Potential of Zero Total Charge of Pt Nanoparticles and Polycrystalline Electrodes with Different Surface Structure: The Role of Anion Adsorption in Fundamental Electrocatalysis. *Electrochim. Acta* **2010**, *55*, 7982-7994.
54. Perry, S.C.; Denuault, G. Transient Study of the Oxygen Reduction Reaction on Reduced Pt and Pt Alloys Microelectrodes: Evidence for the Reduction of Pre-Adsorbed Oxygen Species Linked to Dissolved Oxygen. *Phys. Chem. Chem. Phys.* **2015**, *17*, 30005-30012.
55. Perry, S.C.; Denuault, G. The Oxygen Reduction Reaction (ORR) on Reduced Metals: Evidence for a Unique Relationship between the Coverage of Adsorbed Oxygen Species and Adsorption Energy. *Phys. Chem. Chem. Phys.* **2016**, *18*, 10218-10223.
56. Andricacos, P.C.; Cheh, H.Y. The Application of Linear Sweep Voltammetry to a Rotating Disk Electrode for the Reversible Deposition of an Insoluble Species. *J. Electrochem. Soc.* **1980**, *127*, 2153-2157.

57. Andricacos, P.C.; Cheh, H.Y. The Application of Linear Sweep Voltammetry to a Rotating Disk Electrode for a Reversible Reaction with Soluble Product. *J. Electrochem. Soc.* **1980**, *127*, 2385-2388.
58. Andricacos, P.C.; Cheh, H.Y. The Application of Linear Sweep Voltammetry to a Rotating Disk Electrode for a First-Order Irreversible Reaction. *J. Electroanal. Chem.* **1981**, *124*, 95-101.
59. Quintana, G.C.; Andricacos, P.C.; Cheh, H.Y. Linear Sweep Voltammetry at a Rotating Disk Electrode for First-Order Quasi-Reversible Reactions. *J. Electroanal. Chem.* **1983**, *144*, 77-85.
60. Fried, I.; Elving, P.J. The Rotating Disk Electrode. Effect of Rates of Rotation and Polarization. *Anal. Chem.* **1965**, *37*, 803-806.
61. Strutwolf, J. Schooller, W.W. Linear and Cyclic Sweep Voltammetry at a Rotating Disk Electrode. A Digital Simulation. *Electroanal.* **1996**, *8*, 1034-1039.
62. Levich, V.G. Physicochemical Hydrodynamics, Prentice-Hall, Englewood Cliffs, N. J., 1962.
63. Conway. B.E. Electrochemical Oxide Film Formation at Noble Metals as a Surface–Chemical Process. *Prog. Surf. Sci.* **1995**, *49*, 331-452.
64. Conway, B.E.; Barnett, B.; Angerstein-Kozlowska, H.; Tilak, B.V. A Surface–Electrochemical Basis for the Direct Logarithmic Growth Law for Initial Stages of Extension of Anodic Oxide Films Formed at Noble Metals. *J. Chem. Phys.* **1990**, *93*, 8361-8374.
65. Wroblowa, H.; Rao, M.L.B.; Damjanovic, A.; Bockris, J.O. Adsorption and Kinetics at Platinum Electrodes in the Presence of Oxygen at Zero Net Current. *J. Electroanal. Chem.* **1967**, *15*, 139-150.
66. Hoare, J.P. Rest Potentials in the Platinum-Oxygen-Acid System. *J. Electrochem. Soc.* **1962**, *109*, 858-865.
67. Hoare, J.P. Oxygen Overvoltage Measurements on Bright Platinum in Acid Solutions I. Bright Platinum. *J. Electrochem. Soc.* **1965**, *112*, 602-607.
68. Schuldiner, S.; Roe, R.M. The Pt/O_2 Electrode in Sulfuric Acid Solution. *J. Electrochem. Soc.* **1963**, *110*, 1142-1146.

69. McIntyre, J.D.E. The Kinetics of Electrode Processes with Coupled Heterogeneous Chemical Catalytic Reactions. *J. Phys. Chem.* **1967**, *71*, 1196-1207.
70. McIntyre, J.D.E. The Kinetics of Heterogeneous Catalytic Electrode Reactions. II. Charge-Transfer Kinetics. *J. Phys. Chem.* **1969**, *73*, 4102-4110.
71. McIntyre, J. D. E. On the Distinction between the Kinetics of Parallel and Heterogeneous Catalytic Electrode Reactions. *J. Phys. Chem.* **1969**, *73*, 4111-4115.
72. Katsouraros, I.; Schneider, W.B.; Meier, J.C.; Benedikt, U.; Biedermann, P.U.; Auer, A.A.; Mayrhofer, K.J.J. Hydrogen Peroxide Electrochemistry on Platinum: Towards Understanding the Oxygen Reduction Reaction Mechanism. *Phys. Chem. Chem. Phys.* 2012, 14, 7384-7391.
73. Sánchez-Sánchez, C.M.; Bard, A.J. Hydrogen Peroxide Production in the Oxygen Reduction Reaction at Different Electrocatalysts as Quantified by Scanning Electrochemical Microscopy. *Anal. Chem.* **2009**, *81*, 8094-8100.
74. Shen, Y.; Traüble, M.; Wittstock, G. Detection of Hydrogen Peroxide Produced during Electrochemical Oxygen Reduction using Scanning Electrochemical Microscopy. *Anal. Chem.* **2008**, *80*, 750-759.
75. Shao, M.; Liu, P.; Adžić, R.R. Superoxide Anion Is the Intermediate in the Oxygen Reduction Reaction on Platinum Electrodes. *J. Am. Chem. Soc.* **2006**, *128*, 7408-7409.
76. Kunimatsu, K.; Yoda, T.; Tryk, D.A.; Uchida, H. Watanabe, M. In Situ ATR-FTIR Study of Oxygen Reduction at the Pt/Nafion Interface. *Phys. Chem. Chem. Phys.* **2010**, *12*, 621-629.
77. Tian, F.; Anderson, A.B. Effective Reversible Potential, Energy Loss, and Overpotential on Platinum Fuel Cell Cathodes. *J. Phys. Chem. C* **2011**, *115*, 4076-4088.
78. Omura, J.; Yano, H.; Watanabe, M.; Uchida, H. Electrochemical Quartz Crystal Microbalance Analysis of the Oxygen Reduction Reaction on Pt-Based Electrodes. Part 1: Effect of Adsorbed Anions on the Oxygen Reduction Activities of Pt in HF, $HClO_4$, and H_2SO_4 Solutions. *Langmuir* **2011**, *27*, 6464-6470.
79. Walch, S.P. Effect of Solvation on the Oxygen Reduction Reaction on Pt Catalyst. *J. Phys. Chem. C* **2011**, *115*, 7377-7391.

80. Chen, J.; Fang, L.; Luo, S.; Liu, Y.; Chen, S. Electrocatalytic O_2 Reduction on Pt: Multiple Roles of Oxygenated Adsorbates, Nature of Active Sites, and Origin of Overpotential. *J. Phys. Chem. C* **2017**, *121*, 6209-6217.
81. Keith, J.A.; Jacob, T. Theoretical Studies of Potential-Dependent and Competing Mechanisms of the Electrocatalytic Oxygen Reduction Reaction on Pt(111). *Angew. Chem. Int. Ed.* **2010**, *49*, 9521-9525.
82. Jerkiewicz, G.; Tremiliosi-Filho, G.; Conway, B.E. Significance of the Apparent Limit of Anodic Oxide Film Formation at Pt: Saturation Coverage by the Quasi Two–Dimensional State. *J. Electroanal. Chem.* **1992**, *334*, 359-370.
83. Kongkanand, A.; Ziegelbauer, J.M. Surface Platinum Electrooxidation in the Presence of Oxygen. *J. Phys. Chem. C* **2012**, *116*, 3684-3693
84. Gómez-Marín, A.M.; Schouten, K.J.P.; Koper, M.T.M.; Feliu, J.M. Interaction of Hydrogen Peroxide with a Pt(111) Electrode. *Electrochem. Commun.* **2012**, *22*, 153-156.
85. Sitta, E.; Gómez-Marín, A.M.; Aldaz, A.; Feliu, J.M. Electrocatalysis of H_2O_2 Reduction/Oxidation at Model Platinum Surfaces. *Electrochem. Commun.* **2013**, *33*, 39-42.
86. Liang, C.C.; Juliard, A.L. Reduction of Oxygen at the Platinum Electrode. *Nature* **1965**, *207*, 69-70.
87. Lovric, M.; Osteryoung, J. Linear Scan Voltammetry at Rotating Disk Electrodes. *J. Electroanal. Chem.* **1986**, *197*, 63-75.
88. Gómez–Marín, A.M.; Feliu, J.M. Pt(111) Surface Disorder Kinetics in Perchloric Acid Solutions and the Influence of Specific Anion Adsorption. *Electrochim. Acta* **2012**, *82*, 558-569.
89. Berná, A.; Climent, V.; Feliu, J.M. New Understanding of the Nature of OH Adsorption on Pt(111) Electrodes. *Electrochem. Commun.* **2007**, *9*, 2789-2794.
90. Miller, S.L.; Orlemann, E.F. Non-Additivity of Polarographic Diffusion Currents with Mixtures of Certain Reducible Species. *J. Am. Chem. Soc.* **1953**, *75*, 2001-2003.
91. Andrieux, C.P.; Hapiot, P; Savéant, J.M. Electron Transfer Coupling of Diffusional Pathways Potential Step Chronoamperometry and Cyclic Voltammetry of Cobalt(II)

Tetraphenylporphyrin and 4-Nitrotolueno in Dimethylformanide Solutions. *J. Electroanal. Chem.* **1985**, *186*, 237-246.

92. Bowers, M.L.; Anson, F.C.; Feldberg, S.W. Dealing with Unequal Diffusivities among Reactants in Kinetic Studies at Rotating Disk and Ring-Disk Electrodes. The Reduction of H_2O_2 as Catalyzed by Co^{II}(cyclam) and Fe(II). *J. Electroanal. Chem.* **1987**, *216*, 249-260.
93. Rongfeng, Z.; Evans, D.H. The Current for a Two-Electron Reaction is not Necessarily Twice that of a One-Electron Reaction. *J. Electroanal. Chem.* **1995**, *385*, 201-207.
94. Jirkovsky, J.S.; Halasa, M.; Schiffrin, D.J. Kinetics of Electrocatalytic Reduction of Oxygen and Hydrogen Peroxide on Dispersed Gold Nanoparticles. *Phys. Chem. Chem. Phys.* **2010**, *12*, 8042-8052.
95. Divisek, J.; Kastening, B. Electrochemical Generation and Reactivity of the Superoxide Ion in Aqueous Solutions. *J. Electroanal. Chem.* **1975**, *65*, 603-621.
96. Sawyer, D.T.; Roberts-Jr, J.J. Electrochemistry of Oxygen and Superoxide Ion in Dimethylsulfoside at Platinum, Gold and Mercury Electrodes. *J. Electroanal. Chem.* **1966**, *12*, 90-101.
97. Roberts-Jr, J.L.; Sawyer, D.T. Activation of Superoxide Ion by Reactions with Protons, Electrophiles, Secondary Amines, Radicals, and Reduced Metal Ions. *Isr. J. Chem.* **1983**, *23*, 430-438.
98. Behar, D.; Czapski, G.; Rabani, J.; Dorfman, L.M.; Schwarz, H.A. The Acid Dissociation Constant and Decay Kinetics of the Perhydroxyl Radical. *J. Phys. Chem.* **1970**, *74*, 3209-3213.
99. Airey, P.L.; Sutton, H.C. Electrochemistry of the HO_2 and O_2^- Radicals under Steady State Conditions Part 2.-The Effect of pH over the Range 0.4 to 11. *J. Chem. Soc. Faraday Trans. 1* **1976**, *72*, 2452-2461.
100. Martínez-Hincapié, R.; Berná, A.; Rodes, A.; Climent, V.; Feliu, J.M. Surface Acid-Base Properties of Anion Adsorbed Species at Pt(111) Electrode Surfaces in Contact with CO_2 Containing Perchloric Acid Solutions. *J. Phys. Chem. C* **2016**, *120*, 16191-16199.

101. Noël, J.-M.; Latus, A.; Lagrost, C.; Volanschi, E.; Hapiot, P. Evidence for OH Radical Production during Electrocatalysis of Oxygen Reduction on Pt Surfaces: Consequences and Application. *J. Am. Chem. Soc.* **2012**, *134*, 2835-2841.

102. Liu, Y.; Wu, H.; Li, M.; Yin, J.-J.; Nie, Z. pH Dependent Catalytic Activities of Platinum Nanoparticles with Respect to the Decomposition of Hydrogen Peroxide and Scavenging of Superoxide and Singlet Oxygen. *Nanoscale*. **2014**, *6*, 11904-11910.

103. Roberts, J.G.; Voinov, M.A.; Schmidt, A.C.; Smirnova, T. I.; Sombers, L.A. The Hydroxyl Radical Is a Critical Intermediate in the Voltammetric Detection of Hydrogen Peroxide. *J. Am. Chem. Soc.* **2016**, *138*, 2516-2519.

104. Bielski, B.H.J.; Richter, H.W. A Study of the Superoxide Radical Chemistry by Stopped-Flow Radiolysis and Radiation Induced Oxygen Consumption. *J. Am. Chem. Soc.* **1977**, *99*, 3019-3023.

105. Blelski, B.H.J.; Allen, A.O. Mechanism of the Disproportionation of Superoxide Radicals. *J. Phys. Chem.* **1977**, *81*, 1048-1050.

106. Gerischer, R.; Gerischer, H. Über die Katalytische Zersetzung von Wasserstoffsuperoxyd an Metallischem Platin. *Z. Phys. Chem.* **1956**, *6*, 178-200.

107. Anderson, A.B.; Albu, T.V. Ab Initio Approach to Calculating Activation Energies as Functions of Electrode Potential Trial Application to Four-Electron Reduction of Oxygen. *Electrochem. Commun.* **1999**, *1*, 203-206.

108. Anderson, A.B.; Albu, T.V. Ab Initio Determination of Reversible Potentials and Activation Energies for Outer-Sphere Oxygen Reduction to Water and the Reverse Oxidation Reaction. *J. Am. Chem. Soc.* **1999**, *121*, 11855-11863.

109. Buess-Herman, C.L.; Gierst, L. Potential Step Chronocoulometry of Dioxygen in Aqueous Alkaline Solutions Saturated with Isoquinoline. *Electrochim. Acta* **1984**, *29*, 303-309.

110. Mitsushima, S.; Koizumi, Y.; Uzuka, S.; Ota, K.-I. Dissolution of Platinum in Acidic Media. *Electrochim. Acta* **2008**, *54*, 455-460.

111. Matsumoto, M.; Miyazaki, T.; Imai, H. Oxygen-Enhanced Dissolution of Platinum in Acidic Electrochemical Environments. *J. Phys. Chem. C* **2011**, *115*, 11163-11169.

112. Ozer, D.; Parashf, R.; Broitman, F.; Mor, U.; Bettelheim, A. Electrocatalytic Reduction of Dioxygen by Cobalt Tetra(4-NN'N''-Trimethylanilinium)Porphyrin. *J. Chem. Soc., Faraday Trans. I,* **1984**, **80**, 1139-1149.

Table of Contents